# Investigation of the Failure Behavior of Bolted Connections under Crash Loads and a Novel Adaption to an Enhanced Abstracted Bolt Model

Florian Schauwecker[1,2], David Moncayo[1], Dr.-Ing. Markus Beck[1]
and Prof. Dr.-Ing. Peter Middendorf[2]

[1] *Daimler AG, Research and Development, Sindelfingen, Germany*
[2] *IFB Institute of Aircraft Design, University of Stuttgart, Germany*

## Abstract

*This study presents a new approach for the modelling of bolted joints in vehicle crash simulations with LS-DYNA. In order to evaluate energy absorption concepts, it is essential to transfer loads between joining parts and to predict the failure behavior of threaded fasteners. For conventional models, the maximum tensile strength or the maximum elongation is considered as a failure criteria. Enhanced bolt models require the comprehension of the physics, the failure behavior as well as the corresponding numerical limitations. Experiments were conducted under three different load types, while the thread-shaft ratio, the clamping length and the bolt diameter were varied. The experimental results are utilized on one hand as a reference to validate conventional models and on the other hand as basis for more detailed models.*

*The investigations demonstrate a significant influence of the thread in the analyzed load cases. Due to the reduced material in this part of the bolt, the stiffness, the maximum tensile strength and the elongation differ through the testing conditions. In addition, the numerical analysis indicates a dependence on the number of elements in the cross-section.*

*Taking these characteristics into account leads to an enhanced failure prognosis with an abstract bolt model. Finally, the current achievements will be used to facilitate the evaluation of crashworthiness concepts at an early stage of development.*

## Introduction

Bolted connections are used in almost all kind of vehicles. They are irreplaceable as detachable connections where an easy replacement of parts is required. Moreover, in passenger cars, bolts are used under crash loads to transmit forces between connected parts as a form-fitting connection. Electric vehicles have a heavy battery attached with bolts to the underbody structure. This modifies the safety requirements of the car and influences the vehicle's structural behavior. An adequate failure prediction of the joints is of major importance for the design of new passive safety concepts.

Several modelling techniques for bolted connections were presented over the last years. In large vehicle models the variance of modeling techniques for bolt connections depend on the need of accuracy and modelling effort. Hence, the modelling technique with a beam representing the bolt itself and the connection to the joining parts with a spider mesh of beam elements is the most common way to model a bolted connection [1], [2]. The pre-/post-processing is simple and the accuracy is sufficient for connections with no expected failure.

Sonnenschein [1] published one of the latest modelling techniques for bolts in large vehicle crash simulation. Spotweld-beams abstract thereby the bolt with a strain based failure criteria. Applying *INITIAL_AXIAL_FORCE_BEAM in a cross-section facilitates the pre-stressing condition in the spotweld-beams. Contact beams around the holes and an automatic general contact enable the transmission of loads between the clamped parts.

Hadjioannou, Stevens and Barsotti [3] extended this modelling technique using Hughes-Liu beams, instead of spotweld beams, with the material model *MAT_PIECEWISE_LINEAR_PLASTICITY. Pre-stressing with Hughes-Liu beams cannot be applied over a cross-section, therefore a thermal contraction is required. Both, Sonnenschein and Hadjioannou et al., presented an approach to model a bolted connection under static and dynamic loading conditions with a beam representing the structural bolt axis.

Narkhede et al [2] studied the influence of pre-tension conditions in the bolt, the bearing stress between the bolt shank and the joining parts as well as the friction between the bolt and the clamped plates. Beam elements depict the structural bolt axis, which is connected to the clamped plates through a spider mesh of discrete spring elements, which perform only in compression. A sliding test is used in order to validate the friction between the bolt and the clamped plates. The correspondent discretization uses a bolt model built with hexahedral solid elements.

Solid bolt models apply also for large vehicle models. The abstraction of the bolt consists of a coarse mesh and the material has no failure criteria. This kind of solid bolt models are used in areas with large deformation, where huge bearing stresses and unexpected contacts to the periphery occur. A failure of the bolt is not expected in these regions, owing to the high ratio between the bolt dimension and the thickness of the clamped sheets. A coarse solid model without bolt failure is hereby sufficient. Modelling bolted connections with solid bolt abstractions has the disadvantage that initial penetrations can occur between the shell edge of the clamped plates and the bolt shank, especially when a node to surface contact is used. A segment based contact *CONTACT_AUTOMATIC_SINGLE_SURFACE with SOFT=2 avoids that problem. Additionally, the shell edge formulation facilitates different edge topologies.

Common bolt modelling techniques use a force based or a strain based failure criteria with a bi- or multi-linear stress-strain-curve, not taking into account damage, to describe the material behavior. In areas with large distortions, these abstractions are not precise enough, since the predicted failure does not correspond to experimental results. Either the contact is lost due to eroding elements, with attached contact beams, or the model does not differentiate between the threaded part and the bolt shank.

This study discusses a novel approach for modelling bolted joints in large vehicle crash simulations. An enhanced bolt model, using solid elements with a GISSMO 3D damage model, is proposed in order to obtain a reaction close to the physical bolt behavior. The investigation contains experiments under tension, shear and combined load to characterize the damage and failure behavior of the bolts. The presented experiments indicate physical phenomena which have a significant influence on the failure behavior, not taken into account in current bolt models. The material properties are captured in a detailed model using an average element length of approximately 0.5 mm. The validation effort builds the basis for a subsequent model development through a coarse solid bolt definition with larger element lengths of around 2.5 mm. The proposed modelling strategy and validation contribute to an enhanced damage and failure behavior within bolt connections, and target to capture an appropriate structural behavior beyond early load stages.

## Experimental Setup

The bolt failure characteristics are analyzed under tensile, shear and combined loads with an individual purpose-designed setup for each load case. All testing devices are designed to mitigate boundary effects from peripheral parts in order to obtain an isolated structural failure within the bolt structure. Further, all experimental setups are suitable for drop tower test, with regard to investigating the failure behavior with dynamic loading conditions.

Hence, every setup definition transforms pressure, acting from top to bottom, into the respectively load condition. The experimental program was conducted with M 6, M 8, M 10, M 12 and M 14 bolts made of carbon steel with property class 10.9. Variation-parameters, beside the load direction and the bolt diameter, are thread-shank ratio and the clamping length. The presented fixtures are modular in design. This facilitates the replacement of worn parts and ensures the possible usage with different bolt diameters. In a first phase, these investigations focus on an appropriate description of the bolt material characteristics, therefore no pre-stress is taken into account.

***Tensile load***

The experimental setup for tensile load consists of two round hardened inserts, two square metal inserts, a mounting frame and a counterpart as illustrated in Figure 1. Exchangeable round inserts are available for every bolt diameter and fit into the square inserts, see Figure 1(b). The bolt and nut clamp the assembled inserts, which slide form-fitting into the mounting frame. The counterpart holds the upper square insert. A tensile load develops within the bolt, when the pressure, from above, acts on the mounting frame. Square brass poles on the inside and brass plates on the sides guide the mounting frame in the counterpart. The screws in the counterpart, shown in Figure 1(e), adjust the brass poles to minimize the friction.

The exchangeable round inserts enable to examine different clamping lengths from 40 mm, 50 mm to 60 mm with the same testing device. The experimental program comprehends also a variation of the thread-shank ration in the grip length. Load cells measure the force in the testing unit while the displacement is measured optically through digital image correlation (DIC).

**(a):** Bolt and nut

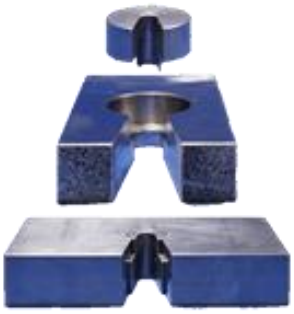

**(b):** Inserts

**(c):** Inserts assembled

**(d):** Mounting frame and assembled inserts

**(e):** Complete assembly

**Figure 1:** Experimental setup for tensile load tests

***Shear***

The shear fixture basically comprises a punch and a counterpart. This setup uses the modularity of the designed concept as well. Figure 2 shows the individual components and the complete assembly. The counterpart holds the bolt, while the punch moves in the middle of the fork. The width of the gap for the shear area is 0.5 mm on each side. Thus, no friction occurs during the test between the clamped parts. This construction leads to a double shearing process, so that the moments interact against each other, which would not be the case with a single-edged connection. The round inserts in the punch and in the counterpart are exchangeable to investigate several diameters with the same setup. Merely for M 6 and M 8 are two separate holes in the counterpart necessary due to the limited availability of bolts applicable with a clamping length of 60 mm. Hence, the clamping length for M 6 is decreased to 40 mm and for M 8 decreased to 50 mm. The area around those holes as well as the round inserts of the punch and the counterpart are hardened. This is necessary, in order to reduce the intrusion of the sharp threaded bolt part in the testing device and thus to prevent an unwitting influence of the periphery.

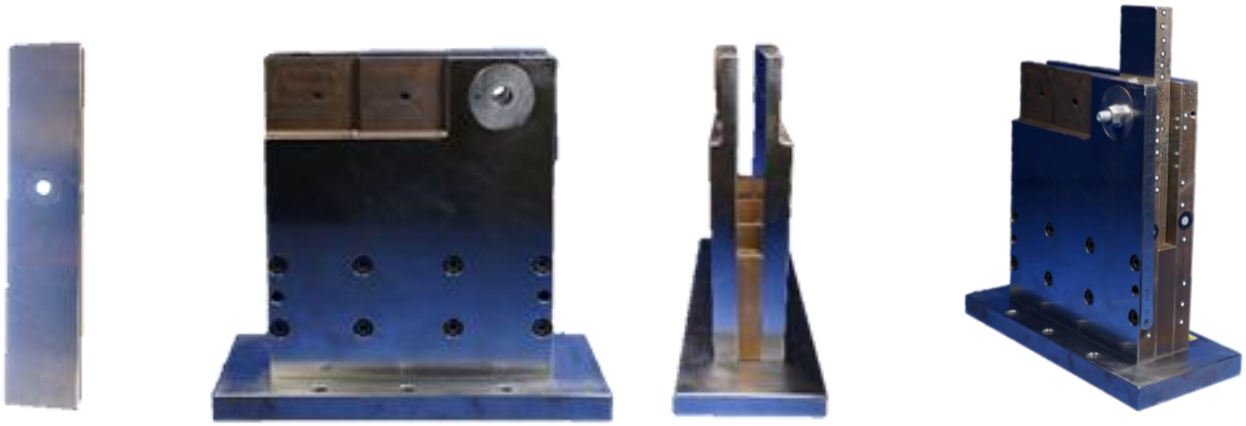

**(a):** Punch **(b):** Counterpart in side and front view **(c):** Complete assembly

**Figure 2:** Experimental setup for shear tests

***Combined load***

Figure 3 illustrates the combined load testing configuration, which uses the same principle as the setup for tensile load, except that the clamped plates are rotated in 45°. The round inserts remain the same for the prior setups; however the square plates as well as the mounting frame and the counterpart are redesigned. This setup uses as well the square brass poles and the brass side plates to guide the mounting frame and to minimize the friction.

**(a):** Mounting frame and assembled inserts **(b):** Counterpart **(c):** Complete assembly

**Figure 3:** Experimental setup for combined load tests

## Experimental Results

The presented results focus on the M 10 bolt category. The same structural characteristics can be expected for the other investigated bolt diameters. The most relevant insights are pointed out and presented in the following descriptions.

***Tensile load***

Since the bolt models do not distinguish between the thread and the shank, the investigations of the thread-shank ratio represent the most remarkable results. The tests include four different free loaded thread lengths (FLTL) 60 mm, 40 mm, 10 mm and 5 mm, while the grip length remained constant 60 mm. The plastic deformation takes place exclusively in the thread, while the shaft only stretches elastically due to the larger cross-sectional area. Consequently, the necking area becomes shorter with the reduction of the FLTL. Steurer [4] describes this effect in detail.

The force-displacement diagram in Figure 4 demonstrates the significant influence of the free loaded thread length. The graphs exhibit a decrease of the displacement while the force level increases with the reduction of the free loaded thread length. The elongation decreases by more than 50%, while the total force level increases slightly by 7% comparing a FLTL of 5 mm to a fully threaded bolt with 60 mm FLTL. The stiffness increases, due to the thread-shank ratio and the different elongations in the shaft and in the thread, respectively.

Two mainly crack patterns categorize the different types of failure. Either the fracture is diagonal, as illustrated in Figure 5 in the upper two rows, or the fracture is flat, as shown in Figure 5 in the lower two rows. The most common case is the diagonal fracture over two to three threads. In extreme cases, the fracture runs over five to six threads as depicted in the second fracture in the upper two rows of Figure 5. Flat fracture patterns are rare and can differ slightly in shape as indicated in the lower two fractures of Figure 5.

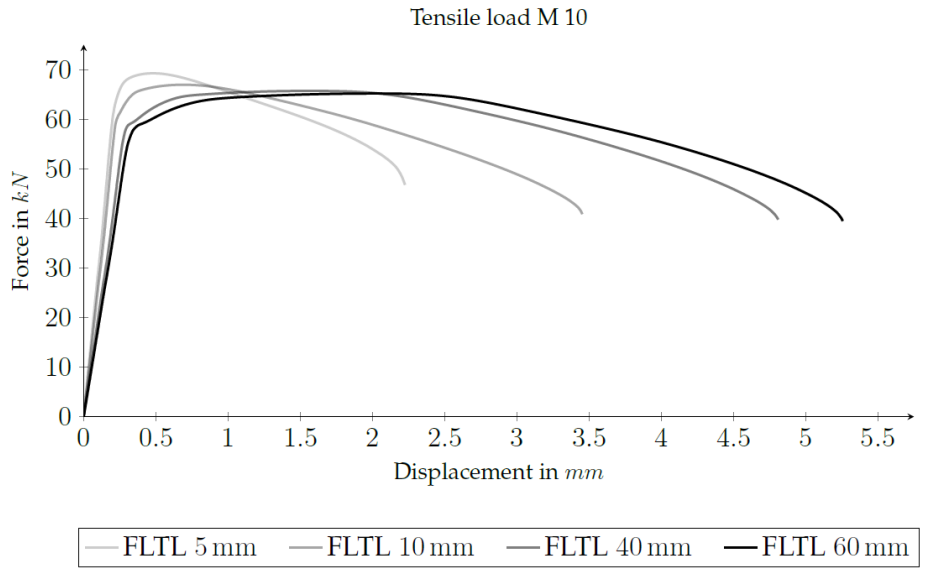


**Figure 4:** Force-Displacement-Diagram of M10 bolts with various thread-shank ratios under tensile load

**Figure 5:** Different crack pattern in the thread under tensile loading

***Shear***

The force-displacement diagram, in Figure 6, exhibits the curve for the shearing in the shank with a continuous line and the shearing in a fully threaded bolt with a dashed line. The thread has a significant influence in this load case. Not only that the force level is lower due to the smaller cross-section area, the material behavior is softer and describes a lower stiffness. The displacement is significantly greater when the thread is located in the shear interface. The plasticization in the shank takes place through a long shear displacement, while the force level gradient remains small.

Figure 7 shows in the upper two pictures the thread before and after the test. The blue area depicts the flat surface at the thread tip, which becomes much wider due to the compression of the thread close to the shearing interface. The compressed thread explains the softer behavior and the longer displacement. The joining partners are often weaker than the bolt, a reason why this behavior usually cannot be observed or isolated. However, there is the possibility, that the thread penetrates the weaker material, which results again in a higher displacement. The sheared cross-section of the shank is illustrated in Figure 7 at the bottom. The smooth surface in the upper area indicates the intrusion depth of around 1 mm, which signalizes the almost constant force level during material plasticization in the diagram.

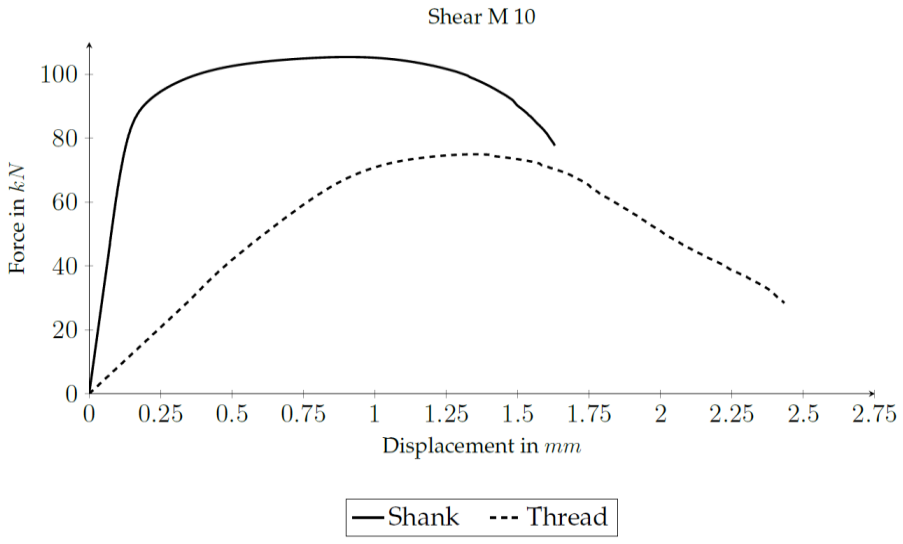


**Figure 6:** Force-displacement diagram of M10 bolts under shear

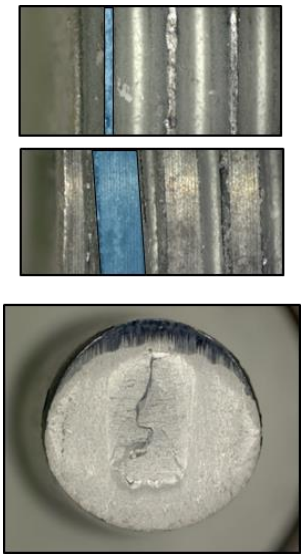

**Figure 7:** Close up of the thread before and after the test (top) and the sheared shank surface (bottom)

***Combined load***

The failure occurs in all test variants in the loading zone between the joining partners, independent of the FLTL and no matter whether the shank or thread is in the shear joint. The solid graph in Figure 8 exhibits the behavior of an M 10 bolt with a FLTL of 5 mm. Failure occurs in the shaft, which makes it partly independent of the free loaded thread length. There is still need to distinguish between the shaft and the thread as the dashed line of a fully threaded M 10 bolt demonstrates. Another effect occurs under combined loading. The stiffness decreases with the thread in the loading area, similar to the observed behavior under shear. However, the displacement and the force level decrease due to the smaller cross-sectional area, as seen under tensile load.

The fracture pattern in Figure 9 is characteristic for fracture in the shaft respectively in the thread. A plateau is formed in the shank from both sides till the crack propagates completely through the material. Interesting is here,

that the crack runs perpendicular to the load direction and not straight to the opposite plateau. The picture of the fracture topology in the thread illustrates the compression of the thread due to the shear loads. The formation of a plateau does not occur in this case. Instead, the thread is strongly deformed.

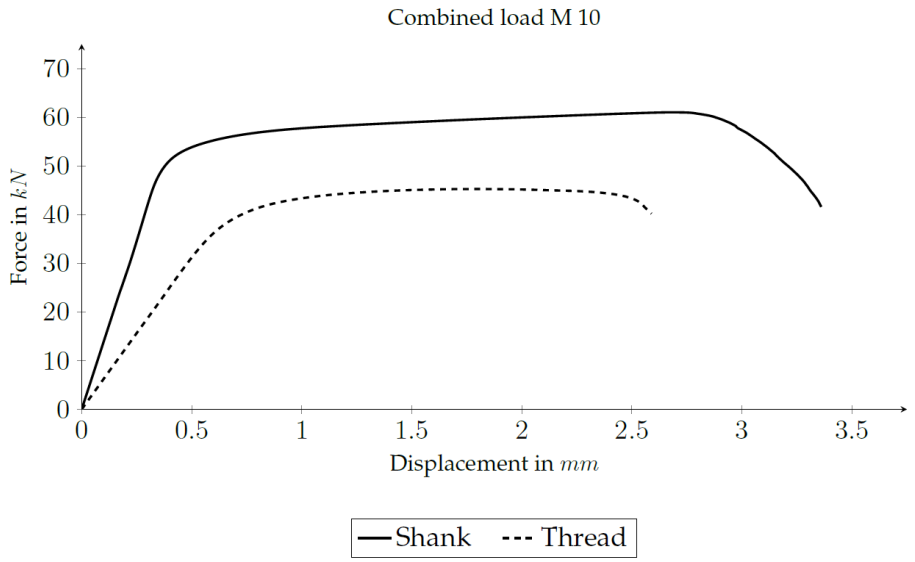


**Figure 8:** Force-displacement diagram of M10 under combined load

**Figure 9:** Fracture characteristics under combined load in the shank (top) and in the thread (bottom)

The characteristics of the plastic deformation resulting under shear and combined loads indicate a micromechanical failure behavior. Capturing these deformations in numerical simulations leads to a complex conflict of the correspondent mesomechanical or macromechanical discretization.

The quotient α in Equation (1) represents the ratio between tensile load and shear. The literature refers to different values for α, form 0.55 to 0.8, depending on the property class and the conducted tests [5]. Shafted bolts are not suitable to examining the correlation between tensile load and shear, due to the influence of the thread-shank ratio under tension and due to larger cross-sectional areas, and thus higher forces, when the shank is sheared. The maximum tensile strength and the maximum shear strength of the presented tests result in an α of 0.58. Equation (2) describes the failure envelope of the bolt for interaction between tensile load and shear. Figure 10 depicts the failure envelope graphically as well as the results under combined load for all bolt diameters. The bolts fail on average close to the loading limit, except M6 which fails beyond the failure envelope.

$$\alpha = \frac{F_{S,max}}{F_{T,max}} \qquad (1)$$

$$\left(\frac{F_T}{F_{T,max}}\right)^2 + \left(\frac{1}{\alpha}\frac{F_S}{F_{T,max}}\right)^2 \leq 1 \qquad (2)$$

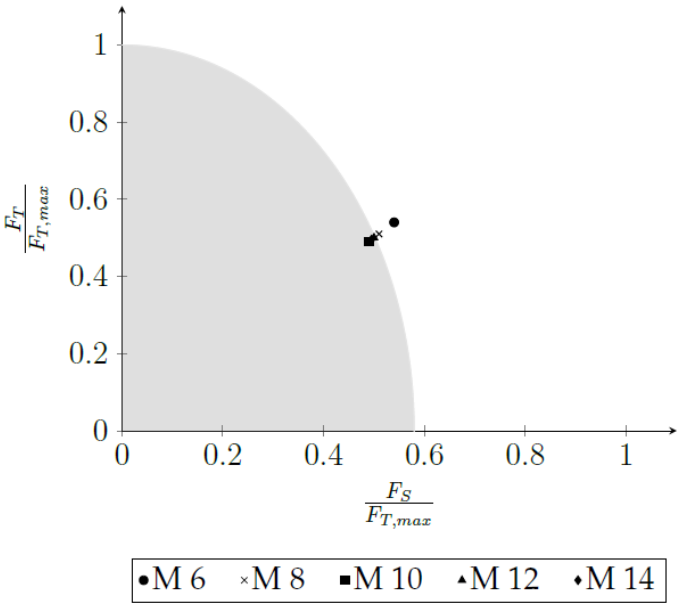


**Figure 10:** Loading area for tension and shear interaction of fully threaded bolts

## Detailed Bolt Model

Renner [5] investigated the tension-shear interaction with M20 bolts of the property classes 4.6, 8.8 and 10.9. She conducted several experiments varying the load angle to the bolt axis between 0°, 15°, 30°, 45°, 67.5°, 90° and 90° with two shear interfaces. The aim of these experiments is the validation of the failure envelopes provided in standards and to propose possible improvements. A numerical detailed bolt model describes the structural behavior of the bolts with an implicit solver. The shank and the inner core of the threaded part are composed of 1 mm hexahedral elements with 20 nodes and quadratic formulation. An automatic mesh generator created tetrahedral elements to abstract the bolt and the thread. The material model uses a multi-linear stress-strain curve, without failure, to depict the bolt behavior and its load paths.

Fransplass, Langseth and Hopperstad [6] presented a study, which analyzes the behavior of threaded M5 rods made of carbon steel with property class 4.6 subjected to combined tension and shear loads under quasi-static and dynamic strain rates. The numerical investigation is conducted with LS-DYNA. The detailed model of the threaded rod uses a characteristic mesh size of approximately 0.075 mm [7]. This magnitude of element size enables enough accuracy to depict the thread geometrically. The automatically generated mesh consists of reduced integrated eight-node hexahedral elements. A thermoelastic-thermoviscoplastic constitutive model *MAT_MODIFIED_JOHNSON_COOK (*MAT_107) describes the material behavior, while a phenomenological fracture criterion, proposed by Cockcroft and Latham [8], takes damage and failure into account.

Figure 11 shows schematically one of the detailed models, used for further investigations, compared to the bolt and nut used in the experiments. The degree of abstraction ranges between a high-resolution detailed model, presented by Renner and Fransplass et al., and a coarse abstraction, which is suitable for large vehicle simulations. The bolt shank and the threaded part are modeled with fully integrated hexahedral eight-node elements (ELFORM2). The target element length for the detailed models is 0.5 mm. The diameter in the shank corresponds with the nominal diameter of the bolt, whereas the diameter in the thread corresponds to the stress cross-sectional diameter of the thread. The precise thread geometry is neglected, due to the selected degree of discretization and the purpose to develop a thread abstraction, which is adaptable for a simplified coarse bolt model with a target element length of around 2.5 mm.

The bolt head and the nut are modeled similarly and have the same geometry. Shell elements with a reduced contact thickness and a physical thickness similar to the bolt diameter represent the contour of the bolt head. These parts use a linear elastic material model without failure. The bolt shank and the threaded part are meshed together, while the nodes at the ends of the bolt are connected over a *CONTACT_TIED_NODES_TO_SURFACE to the head and nut, respectively.

**Figure 11:** The detailed bolt model compared to the real bolt

The cross-sections of the respective bolt diameters are presented in Figure 12. Renner and Fransplass et al. used a perfectly squared pattern of hexahedral elements in the bolt core, which leads to large distortion in the transition to a round pattern. Small element lengths at the corners and high aspect ratios of the elements are the result. A mesh convergence study is conducted to obtain a smooth transition from the squared pattern to a round outer contour. An additional element row is added to the circular cross-section contour to obtain the nominal diameter for the shanked part of the bolt.

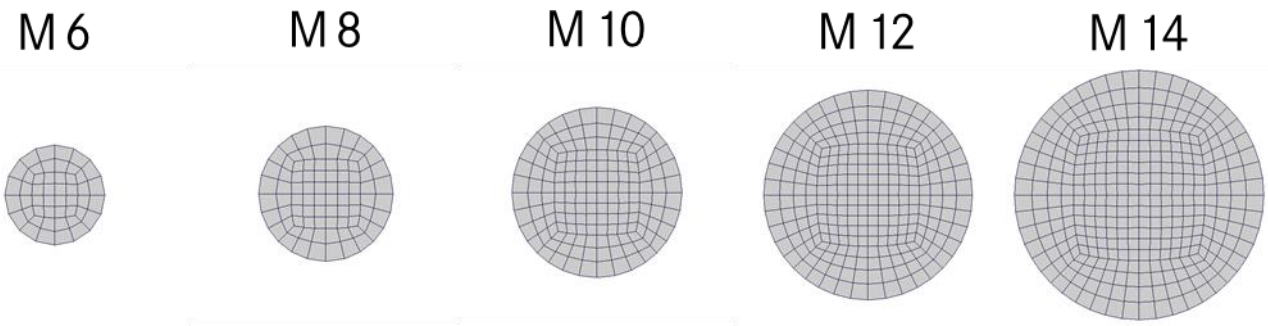


**Figure 12:** Thread cross-sections of the detailed models from M 6 to M 14

The international standard ISO 898-1 [9] defines the requirements for a bolt of the property class 10.9, in which the minimum yield stress is defined as $R_{p0.2}$ = 940 MPa and the minimum tensile strength is defined as $R_m$ = 1040 MPa. This properties correspond with a complex phase steel CP 1000. A material card for the CR780Y980T-CP, provided from the material database of the Daimler AG, shows similar characteristics as it is required for the property class 10.9. The yield stress and the tensile strength of the material card are $R_{p0.2}$ = 942 MPa and $R_m$ = 1037 MPa. The material card uses the material model *MAT_PIECEWISE_LINEAR_PLASTICITY (*MAT_24) to describe the yield curve and additionally *MAT_ADD_EROSION to take damage and failure through the GISSMO damage model into account. The validation of the material card was carried out with an A10 small tensile specimen test, a notched tensile specimen test with a notch radius of 4 mm, a shearing test under 0° and a shearing test under 45°, all with an element length of 0.5 mm. Effelsberg et al. [10] described the tests and the process of the validation for a GISSMO damage model in detail. The element size for the validation of the material card is another reason for the choice of a 0.5 mm element length in the detailed model. In addition, a regularization from 0.5 mm to 10 mm is available for this material card. However, the material card is only validated for a plane stress assumption with shell elements (ELFORM16). The GISSMO failure criterion is hereby constant for all lode parameter from -1 to 1, when the material card is applied to solid elements. The segment based contact *AUTOMATIC_SINGLE_SURFACE with SOFT=2 is used for contact between all parts and in all simulations. The presented numerical investigation is done for the tensile and the shear test.

***Tensile load***

The tensile load setup is reduced to the inserts. Figure 13 illustrates the tensile load simulation model for M10 bolts. Rigid shell elements with a contact thickness of 0.1 mm depict the surface of the round and the square inserts. This is done to save computing power and time. The upper round and square inserts are fixed in all translational and rotational degrees of freedom. A constant velocity along the bolt axis applies to the lower inserts. A cross-section through the bolt shank provides the force data. The difference between two history nodes at each end of the shank results in the displacement.

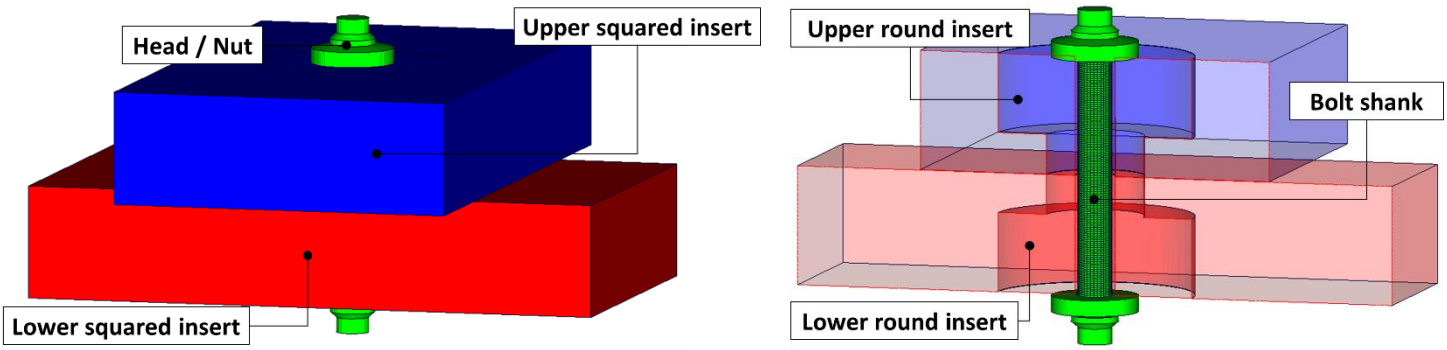


**(a):** Tensile model in isometric view **(b):** Tensile model in cut view

**Figure 13:** Model for tensile load simulation

***Shear***

The punch and the relevant section of the counterpart are abstracted to model the shearing test as shown in the Figure 14(a). Rigid shell elements, with the same properties as used for the tensile test, depict the contour of the setup parts. Figure 14(b) illustrates the bolt and the two shear areas between the punch and the counterpart in a close-up view. Both shear joints have a width of 0.5 mm, similar to the test setup. Thus, the friction can be neglected between the punch and the counterpart yet defined in the contact, because of the interaction between the setup parts and the bolt. A history node on the punch provides the displacement in these models. The force measurement of the shear load in the bolt itself is complex. A cross-section parallel to the bolt axis and perpendicular to the load direction leads to inaccurate results. Instead, either the contact force between the bolt and its surrounding or the reaction forces in single point constraints (SPC) at the bottom could measure the force. However, the oscillations are quite high with these techniques. The model in Figure 14 uses a third method.

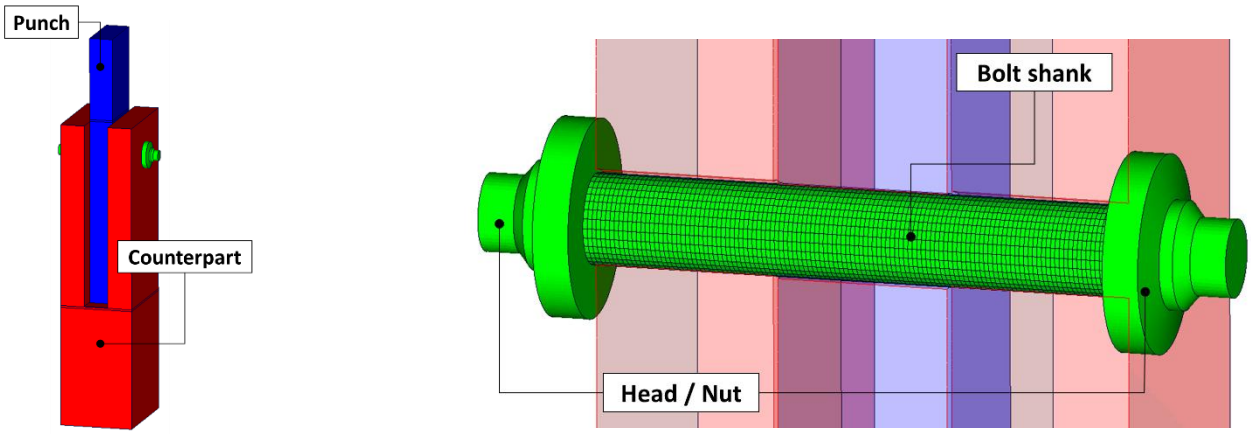


**(a):** Shear model in isometric view **(b):** Shear model in close-up cut view

**Figure 14:** Model for shear simulation

In this model, three element rows, each 0.5 mm high, separate the punch as well as the counterpart in two parts. These element rows are non-rigid, but with an elastic material model of high stiffness and a wall thickness of 30 mm. The upper rigid body of the punch moves with a constant velocity perpendicular to the bolt axis, while the remaining translational and rotational degrees of freedom are blocked. The lower rigid part of the punch has no blocked degrees of freedom and is connected to the non-rigid elements. Under loading, the rigid bodies are compressing these elastic element rows and the force is measured through a cross-section in the middle element row. The similar method is used in the counterpart, while the lower rigid body of the counterpart is constrained and the upper part moves freely.

## Simulation Results

***Tensile load***

Figure 15 shows the force-displacement diagrams for M 10 bolts with various free loaded thread lengths under tensile load. The graphs exhibit the results with the two-dimensional material card for a CP 1000 complex phase steel mentioned above. The red solid curves describe the behavior of the numerical bolt models, which underestimates the force level of the experiments. The parameters of the material card are almost equal to the minimum requirements of the material properties for 10.9 bolts [9]. Material parameter scatter for every bolt, due to the fact that manufacturers purchase raw material from various suppliers and due to the manufacturing process whose parameter cannot be kept constant for every bolt. For this reason, the yield stress and the tensile strength are higher than the required minimum of the standard. However, the maximum tensile stress is limited by the Vickers hardness [9]. The yield stress should not exceed $R_{p0.2}$ = 1090 MPa and the maximum tensile stress is defined as $R_m$ = 1190 MPa, additionally the yield stress and the tensile strength have to be in a certain ratio to each other. After all, the graphs in Figure 15 prove that the detailed bolt models depict the material behavior, owing to the distinction between the cross-sectional area of the shaft and the stress cross-sectional area in the thread. The force level increases while the displacement decreases with reduction of the free loaded thread length, corresponding with the physical bolt behavior. The models next to the respective graph are displayed in a cut view. Low plastic deformations are white and high plastic deformations are red colored. The figures present the models right before rupture occurs. The plastic deformation and thereby the localization occurs in the middle of the threaded part and moves closer to the nut with an increase of the thread-shank ratio. As the figures demonstrate, the necking process needs enough space in axial direction for its usual ductile behavior. Reducing the constriction area leads to an increase in the force level and a reduction of the elongation. The numerical replication indicates this brittle behavior in a reduction of the plastic deformation, as seen in Figure 15(c) and Figure 15(d).

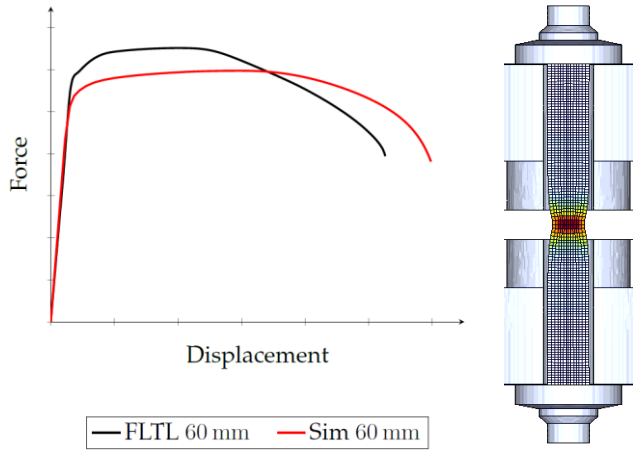


**(a):** Force-displacement diagram and numerical model for a free loaded thread length of 60 mm

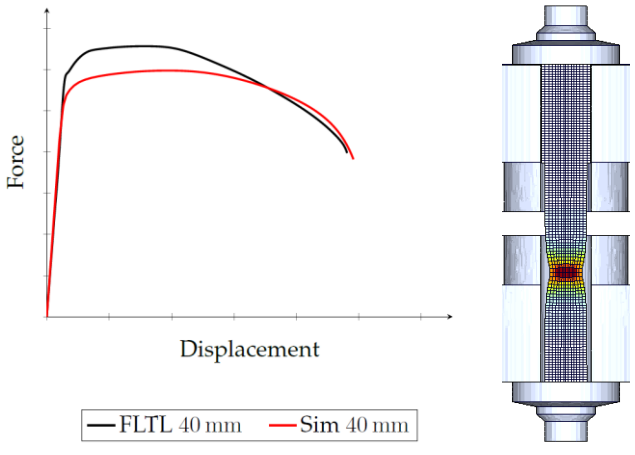


**(b):** Force-displacement diagram and numerical model for a free loaded thread length of 40 mm

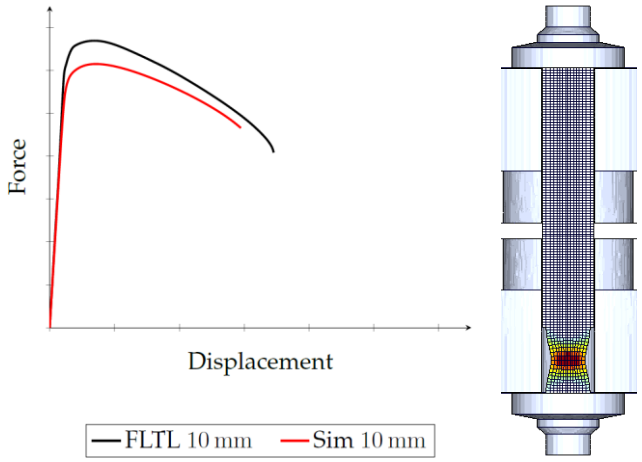


**(c):** Force-displacement diagram and numerical model for a free loaded thread length of 10 mm

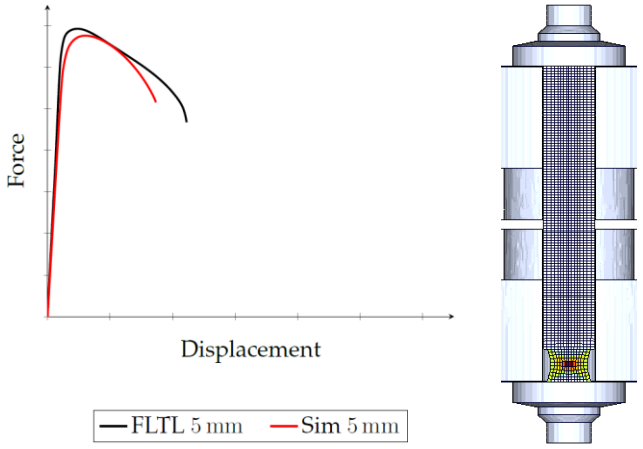


**(d):** Force-displacement diagram and numerical model for a free loaded thread length of 5 mm

**Figure 15:** Force-displacement diagrams of the tension load simulation with various free loaded thread lengths and their related numerical models at rupture regarding plastic strain

***Shear***

Figure 16 shows the simulation results of the shear test compared to the experimental results in a force-displacement diagram. The simulation is as well conducted with the previously mentioned material card of a CP 1000 steel. The material behavior in the shank follows the experimental results till the maximum force level. The bolt begins to fail after approximately 2 mm displacement, while the bolt fails in the experiment already at around 1.5 mm. As Figure 17 illustrates, the elements in the shear interface are strongly distorted at a displacement of 3 mm, due to the definition of the critical plastic strain curve and the failure strain curve at the triaxiality close to shear ($\eta = 0$) in the GISSMO damage card. A high plastic failure strain for compression is selected, because a material failure is not expected under this loading conditions. Furthermore, only certain points of the failure envelope are defined due to the extensive evaluation of the damage parameter under various failure modes, discussed before [10]. LS-DYNA interpolates linearly between the defined coordinates. The ductile behavior of the elements is seen in the force-displacement curve beyond 2 mm. The force decreases slowly, due to these large elongations in the elements.

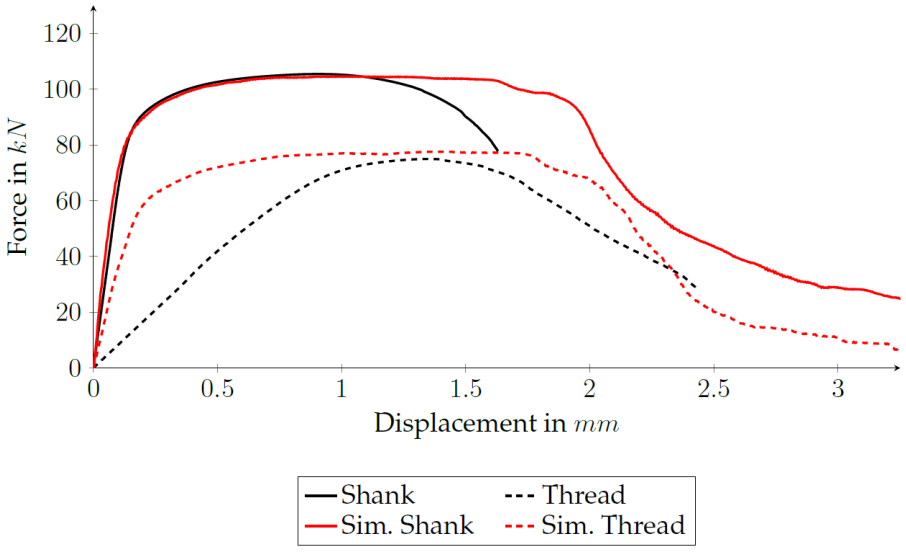


**Figure 16:** Force-displacement diagram of the shear simulation compared to the experimental results

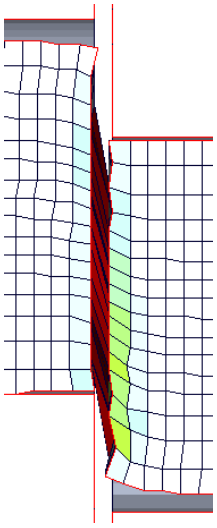

**Figure 17:** Close-up of the shear interface in the shank at 3 mm displacement regarding plastic strain

The model for shearing, with the stress cross-sectional diameter, reaches the same force level as the experimental curve. However, the bolt stiffness is higher in the simulation than in the experiment, due to the neglected thread. An adequate thread modelling has yet to be found.

The critical plastic strain and the failure strain of the three-dimensional GISSMO damage card are investigated in order to capture the failure behavior under shear more precisely. Figure 18 exhibits the results of the adaptions in a force-displacement diagram. The elements fail at a shorter elongation, which leads to an earlier decrease of the force, as shown in Figure 18. The simulation model for shearing in the shank follows thereby the experimental curve till rupture occurs. Figure 19 illustrates the plastic strain again at 3 mm displacement and with the same range of colorization. The elements are already eroded at this point and the bolt fractures under shear.

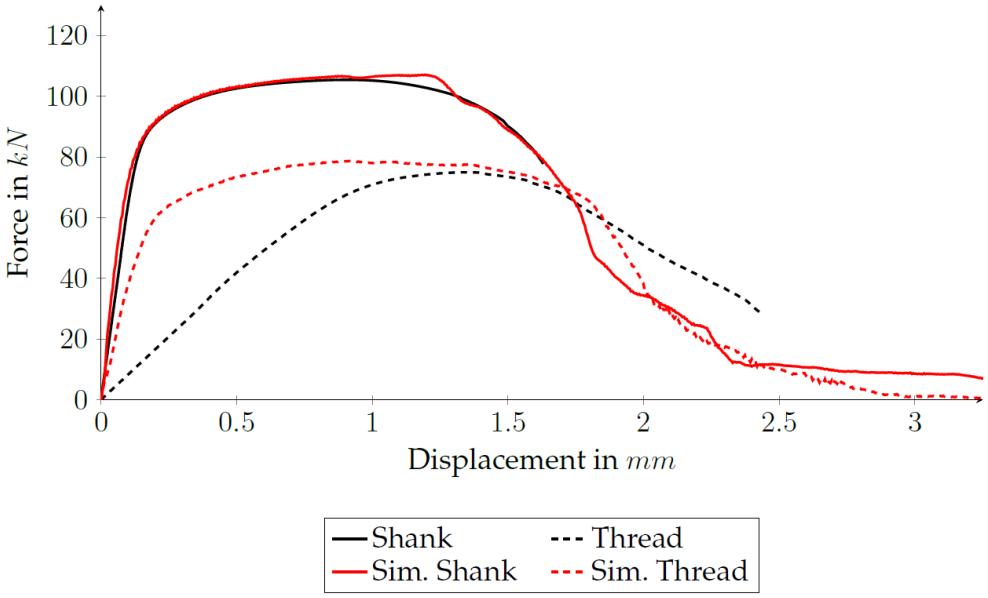


**Figure 18:** Force-displacement diagram of the shear simulation compared to the experimental results

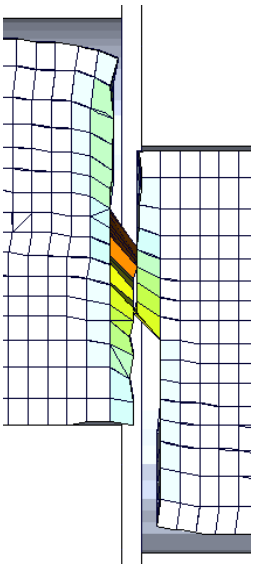

**Figure 19:** Close-up of the shear interface in the shank at 3 mm displacement regarding plastic strain

## Conclusion

A characterization of the bolt material behavior is conducted with purpose-made setups under tensile, shear and a combined loads. The physical phenomena, which are not covered through simplified bolt models, are analyzed in detail. The experimental results under tension demonstrate that the elongation and the maximum force level depend on to the thread-shank ratio. The bolts behave more brittle when the free loaded thread length becomes shorter. A detailed bolt model, related to a material card of a CP 1000 complex phase steel, depicts this behavior in the simulation through a distinction between the cross-sectional area in the thread and in the shank.

The shear test in the thread shows a lower maximum force level than the shear test in the shank due to the smaller cross-sectional area. The thread is compressed during the shear test, which leads to a decrease of the stiffness and an increase of the total elongation. The simulation results for shearing in the thread exhibit that the detailed model reaches the same force level as the experiment, however the stiffness and the total elongation deviate due to the neglected thread geometry. The stiffness and the maximum force level are captured by the detailed model, when the shank is in the shear joint. Further, the results point out that the elongation is captured more precise, with an adaption of the critical plastic strain and the failure plastic strain for a shear stress state.

Under combined tensile and shear loads, the experimental results show again a decrease of the stiffness and the force level when the thread is in the loading area. In this load case, however, the elongation is decreasing as well, compared to the elongation when the shank is in the loading area. A comparison to the simulation is not presented for this loading case.

The results indicate the major importance to differentiate between the respective cross-sectional areas to capture the physical phenomena in an appropriate manner. An abstraction for the thread influence under shear loads has yet to be found in further investigations. The generated insights of the physical phenomena and the numerical limits lead further to the development of an enhanced bolt abstraction suitable for large vehicle simulations.

## References

[1] U. Sonnenschein, Modelling of bolts under dynamic loads, 7. LS-DYNA Anwenderforum, Bamberg, 2008

[2] S. Narkhede, N. Lokhande, B. Gangani, G. Gadekar, Bolted Joint Representation in LS-DYNA to Model Bolted Pre-Stress and Bolt Failure Characteristics in Crash Simulations, 11th International LS-DYNA Users Conference, Dearborn MI USA, 2010

[3] M. Hadjioannou, D. Stevens, M. Barsotti, Development and Validation of Bolted Connection Modelling in LS-DYNA for Large Vehicle Models, 14th International LS-DYNA Users Conference, Detroit MI USA, 2016

[4] A. Steurer, Trag- und Verformverhalten von auf Zug beanspruchten Schrauben, Zürich, 1996

[5] A. Renner, Zug-Abscher-Interaktion bei Schrauben im Stahlbau, Darmstadt, 2016

[6] H. Franzplass, M. Langseth, O. S. Hopperstad, Experimental and numerical study of threaded steel fasteners under combined tension and shear at elevated loading rates, International Journal of Impact Engineering, 2015

[7] H. Franzplass, M. Langseth, O. S. Hopperstad, Numerical study of the tensile behavior of threaded steel fasteners at elevated rates of strain, International Journal of Impact Engineering, 2013

[8] MG. Cockcroft, DJ. Latham, Ductility and the Workability of Metals, 1968

[9] International standard, ISO 898-1, mechanical properties on fasteners made of carbon steel and alloy steel – Part 1: bolts, screws and studs, Brussels: European Committee for Standardization, 1999

[10] J. Effelsberg, A. Haufe, M. Feucht, F. Neukamm, P. Du Bois, On parameter identification for the GISSMO damage model, 12th International LS-DYNA Users Conference, 2012